Integrating Materials and Manufacturing Innovation (2024) 13:857–865
https://doi.org/10.1007/s40192-024-00383-1

THEMATIC SECTION: 2ND WORLD CONGRESS ON ARTIFICIAL INTELLIGENCE IN MATERIALS & MANUFACTURING

Equivariant Neural Networks for Controlling Dynamic Spatial Light Modulators

Sumukh Vasisht Shankar[1] · Rui Wang[2] · Darrel D'Souza[3] · Jonathan P. Singer[3] · Robin Walters[1]

Received: 3 September 2024 / Accepted: 31 October 2024 / Published online: 22 November 2024

Abstract
Spatial light modulators (SLMs) are devices that are capable of manipulating incident light by passing it through an array of phase/intensity altering pixels. A recent alternative design involves creating a phase mask by directing a thin film of fluid with thermocapillary forces generated by a controlled temperature map. However, it is difficult to determine the input temperature signal necessary to induce a given height profile. The relationship between temperature and height is given by the thin film equation, a fourth-order nonlinear PDE, which is difficult to solve numerically. To address this problem, we train deep neural networks to directly solve the inverse problem, mapping from the desired height profiles to the needed temperature patterns. We design novel equivariant networks incorporating scale and rotation symmetry of the underlying thin film equation. We demonstrate the effectiveness of equivariant models for learning the complex relationship between input temperature signals and the resulting light patterns, showing they are more accurate than non-equivariant baselines and very computationally efficient. This work has implications for a range of applications, including high-power laser systems, and could lead to more efficient and effective ways to deploy the process of modulation of light in SLMs in a variety of applications.

Keywords Machine learning · Thin film equation · Spatial light modulator · Equivariant neural networks

Introduction

Deep learning (DL) has emerged as a powerful tool for many scientific fields, including material science [1], climate science [2], biology [3], and neuroscience [4]. Recent works have shown that DL can generate realistic predictions and significantly accelerate the simulation of physical systems relative to numerical solvers, from turbulence modeling to weather prediction [5]. Within materials science, DL has demonstrated efficiency in analyzing and understanding intricate material structures, design, and properties [6, 7]. Traditional methods for predicting changes in material properties can be time-consuming due to their reliance on extensive experimentation, intricate numerical analyses, and the iterative nature of the design-make-test-analyze cycle. DL offers a more efficient approach by directly predicting material properties based on their chemical composition and other factors and bypassing slow numerical methods [8, 9].

In this paper, we employ DL to forecast the temperature profile needed to generate a specific reflected light pattern using a thermocapillary dewetting-based dynamic spatial light modulator (SLM) [10]. SLMs modulate light beams by utilizing fluid films whose heights can be adjusted through temperature gradients. The relationship between temperature and height is governed by the thin film equation [11–13]. It is a fundamental equation in the study of thin film lubrication and wetting phenomena, characterizing the spatial and temporal behavior of thin fluid films on solid surfaces. By numerically solving the equation, one can perform forward modeling of the system, determining the evolution of the height profile of the fluid over time in response to

Sumukh Vasisht Shankar and Rui Wang have contributed equally to this work.

✉ Sumukh Vasisht Shankar
vasishtshankar.s@northeastern.edu

[1] Khoury College of Computer Sciences, Northeastern University, Boston, MA, USA

[2] Department of Electrical Engineering and Computer Science, Massachusetts Institute of Technology, Cambridge, MA, USA

[3] School of Engineering, Rutgers University, New Brunswick, NJ, USA

temperature. More critical for controlling the SLM is the inverse problem, to determine the temperature profile when provided a target height profile. Forward modeling is computationally expensive, and the inverse problem is even more difficult. Here, we demonstrate that DL models can efficiently solve both problems.

Conventional neural networks require a large amount of data to correctly capture the correlation between the height and corresponding temperature profiles but obtaining substantial real experimental data is challenging. Thus, we propose to incorporate the rotational, translational, and scale symmetries of the thin film equation into convolutional neural networks to build equivariant networks. Equivariant models that preserve desired symmetries not only enjoy favorable sample complexity compared with data augmentation but are also robust to distributional shifts by symmetry group transformations [14, 15]. Specifically, our contributions include:

- We study the problem of predicting the input temperature profile required to induce a given height profile in dynamic SLMs with DL.
- We generate a two-dimensional simulated dataset by numerically solving the thin film lubrication equation.
- We demonstrate that incorporating rotational and scale symmetries enhances accuracy, generalization ability, and sample efficiency.
- We propose a novel roto-scale-equivariant model that can preserve rotation and scale symmetries concurrently.

Application Description

SLMs and Thermocapillary Dewetting

Dynamic SLMs (Fig. 1) are devices that can precisely alter incident light by tuning either the phase shift and/or the reflectivity/transmission of an array of pixels in parallel. They are used in optics to control the behavior of light and are used for a number of applications like projectors, laser beam shaping, beam front aberration, etc. They can also be used to manipulate the properties of microscopic particles (i.e., optical tweezing) and materials (i.e., lithography) by applying different light patterns to them.

Conventional dynamic SLMs, which employ liquid crystal optics, are normally incompatible with high-powered sources due to the heating that invariably results from even slight optical absorption. To address this issue, [10] presents the usage of thermocapillary dewetting to dynamically

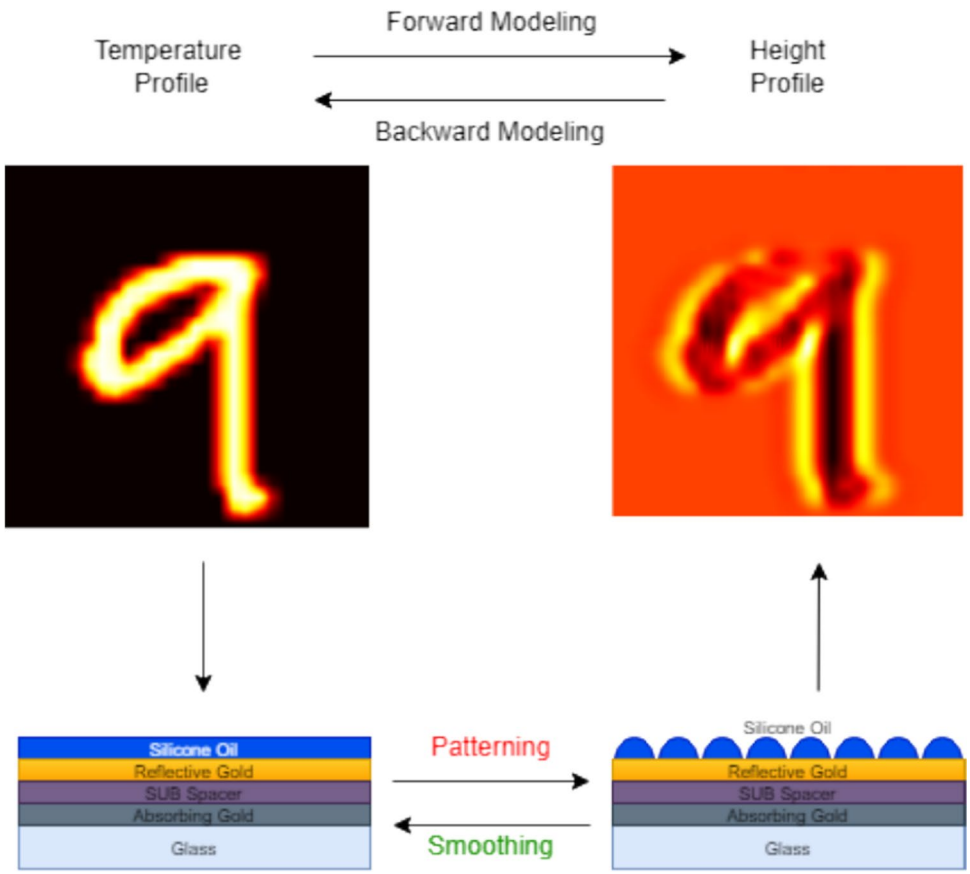

Fig. 1 Schematic of multilayer SLM showing forward and backward modeling tasks

control the thickness of a thin viscous, transparent film positioned on a high-power mirror. This film, when used with an SLM, results in the incident beam of light being phase-shifted and focused based on the height map (pattern) of the film. Due to the low thickness and optical absorption, heat generation is negligible.

Thin Film Equation

The thin film lubrication equation is a partial differential equation that describes the behavior of a thin fluid film on a solid surface. It is a fundamental equation in the study of thin film lubrication and wetting phenomena.

The thin film lubrication equation is a simplified form of the Navier–Stokes equations that govern fluid motion. It describes the evolution of the thickness profile of the fluid film as a function of time and position. The equation takes into account the balance between the viscous forces within the fluid and the intermolecular forces between the fluid and the solid surface.

Mathematically, the thin film equation can be written as,

$$\frac{\partial h}{\partial t} = -\nabla \cdot (q) \tag{1}$$

where h is the thickness of the film, t is time, and q is the flux of fluid in the x and y directions.

The driving force of thermocapillary dewetting [4, 12, 16] is the thermocapillary shear $\tau = \beta \nabla T$. The evolution of the height profile of the film is described by the thin film lubrication equation,

$$\frac{dh}{dt} = -\nabla \cdot \left(\frac{h^2 \beta \nabla T}{2\mu} + \frac{h^3}{3\mu} \left(v \nabla^2 h + \frac{dV}{dh} \right) \right) \tag{2}$$

where μ is the fluid viscosity, h is the film thickness, and V encapsulates surface interactions. When the film is heated, it becomes thin in the heated areas and thick in the surrounding areas, which leads to the formation of trench and ridge structures. [10] explains the real-world experimental setup along with images.

Symmetries of Thin Film Equation

The thin film equation is invariant under the following transformations. Various papers [14, 17, 18] in the past have performed Lie symmetry analysis for the thin film equation and have showcased the solutions for different classes of the thin film equation. Individually each of these types of transformations generates a group of symmetries of the system.

- Space Translation:

  $T_y^{\text{space}} h(x,t) = h(x-y,t), y \in R^2$

- Time Translation:

  $T_y^{\text{time}} h(x,t) = h(x,t-s), s \in R$

- Rotation:

  $T_R^{\text{rot}} h(x,t) = h\left(R^{-1}x, t\right), R \in SO(2)$

- Scaling:

  $T_\lambda^{\text{scale}} h(x,t) = h\left(x\lambda^{\frac{-1}{4}}, t\lambda^{-1}\right), \lambda \in R_{\geq 0}$

Relevance of AI to Material Science Applications

Modeling physical dynamics is crucial not only for our application but for diverse fields like physics, epidemiology, and molecular dynamics. Traditional methods rely on numerical models based on complex differential equations representing physical laws. These techniques are computationally expensive and require manual engineering in each application. DL has also shown significant speed up in solving PDEs that govern physical processes [19]. This is because DL can directly estimate PDE solutions or predict system future states, eliminating the need for numerical integration [20, 21].

Physics-informed DL [1, 2] is a class of approaches that integrates mathematical principles or prior physics knowledge into the design of neural nets to develop predictive models for complex physical systems. It aims to take the best from both types of approaches to better solve scientific problems.

For material science, in particular, physics-informed DL methods have several advantages over traditional modeling approaches, including capturing complex nonlinear relationships between material properties, processing conditions that may be difficult to model using traditional methods, incorporating physical principles into the model, which ensures that the predicted results are physically meaningful, and reducing the amount of experimental data needed to develop accurate models.

Integrating symmetries in neural networks significantly enhances their generalizability and sample efficiency. Deep models, when designed to be equivariant or invariant to group transformations, are more robust to distribution shift and require fewer data samples to train. While equivariant DL models have achieved remarkable success in computer vision domain [22–26], the study of equivariant nets in learning dynamical systems is newer but is becoming

increasingly popular [9, 27–29]. Part of the motivation for incorporating symmetries comes from the pivotal role they play in physics. Noether's law, for instance, establishes a connection between conservation laws and symmetries. This suggests that neural networks that respect symmetries generate predictions that are more physically accurate [27].

AI Approach and Innovation

Problem Formulation

In this paper, our main objective is the backward task of finding the temperature profile (represented as T in Eq. 2) required to produce a desired height profile (denoted as H in Eq. 2). We also demonstrate our model can learn the forward task, predicting the height profile for a given temperature profile, to show the model can capture system dynamics. For the backward task, we train models using height profiles to predict temperature profiles. For the forward task, we use temperature profiles to predict height profiles.

Equivariant Convolution Neural Networks

Equivariant neural networks are a class of deep neural networks that are designed to preserve geometric symmetries and behave in a way that is consistent with the transformations of the input data, such as rotations, translations, and reflections.

Definition 1: A function $f : X \to Y$ can be described as respecting the symmetry coming from a group G using the notion of equivariance. We say a function f is *G-equivariant* if

$$f(g(x)) = g(f(x)) \tag{3}$$

for all $x \in X$ and $g \in G$. The function f is *G-invariant* if $f(gx) = f(x)$. For example, G can represent the group *SO(2)* of all possible 2D rotations.

Figure 2 illustrates the concept of rotational equivariance. In the setting of our experiments, f approximates the map between the temperature profile and height profile. We first provide a concise overview of the two types of equivariant networks we utilize in our experiments: G-convolution and G-steerable CNN.

G-Equivariant Group Convolution

[22] defines a generalization of CNNs to an arbitrary symmetry group G. Taking $G = Z^2$, the group of discrete translations, recovers CNNs. Group convolution takes as input a c_{in}-dimensional feature map $f : G \to R^{C_{in}}$ and convolves it with kernel $\Psi : G \to R^{C_{out}XC_{in}}$ over a group G,

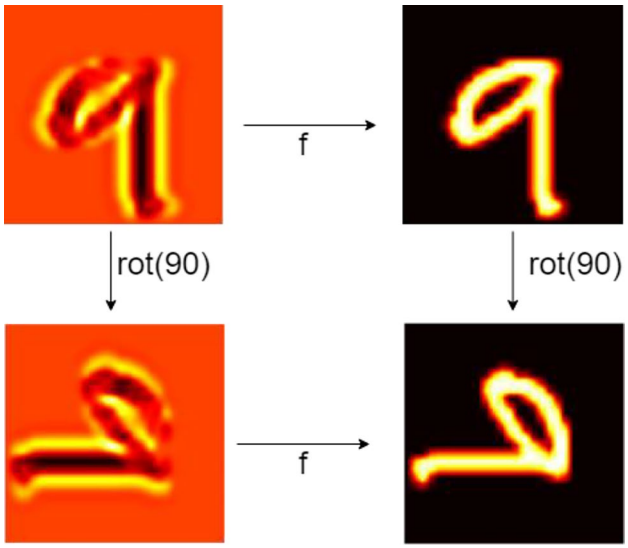

Fig. 2 Backward modeling task of predicting the temperature profile required for producing a given height profile. Rotational equivariance of this backward task mapping temperature to height with respect to g = rot(Π/2)

$$\left[f \star_G \Psi\right](g) = \sum_{h \in G} f(h)\Psi\left(g^{-1}h\right) \tag{4}$$

Steerable CNNs

[15] utilizes steerable filters from signal processing to design equivariant convolutional layers. Let f be the input feature map $f : R^2 \to R^{C_{in}}$ with group $H \subset O(2)$ acting on R^2 by matrix multiplication and on the feature space $R^{C_{in}}$.by ρ_{in}. Also fix an H-action ρ_{out} on $R^{C_{out}}$. Let $\Phi : R^2 \to R^{C_{out}XC_{in}}$ be a kernel, the standard 2D convolution $f \star_{R^2} \Phi$ is H-equivariant and R^2-translation equivariant when

$$\Phi(hx) = \rho_{out}(h)\Phi(x)\rho_{in}\left(h^{-1}\right) \forall h \in H \tag{5}$$

Solving for a basis of solutions to Eq. 5 gives an equivariant kernel basis $\{\Phi_l\}_{l=1}^{L}$. The kernels we use in Steerable CNNs are linear combinations of these basis with trainable coefficients $\Phi = \sum_{l=1}^{L} \omega_l \Phi_l$.

For rotation symmetry, we use the rotational equivariant ResNet (*RotEq-ResNet*) and U-Net (*RotEq-U-Net*) architectures from [27]. For scale symmetry, we employ the scale-equivariant steerable network (*SESN*) from [30]. SESNs use the concept of steerable filter parametrization which allows for scaling without the need for tensor resizing. They are equivariant to scale transformations with arbitrary discrete scale factors. They do not rely on any image resampling techniques during training. Since we directly learn the

transformation between the temperature profile and height profile, we do not need to consider the change of time under scaling transformation. Thus, it is only essential to ensure the model's equivariance when scaling spatial dimensions.

Roto-Scale-Equivariant Convolution

Unlike many existing studies that focus on one symmetry group, we propose an approach that ensures simultaneous rotation, translation, and scale equivariance. To make convolution equivariant to both rotation and scaling transformations, we define a novel architecture *RotSc* which combines rotation steerable convolution [15] with scaling group convolution [23]. Utilizing the ESCNN library [31], we can obtain a rotationally equivariant steerable kernel basis $\{\Phi_l\}_{l=1}^{L}$ for different input and output representations. We then replace the unrestricted kernels Ψ in the scale group convolution [23] with those that are rotationally equivariant. The Φ we use in the following is already

a linear combination of rotational equivariant kernel basis with trainable weights $\Phi = \sum_{l=1}^{L} \omega_l \Phi_l$.

Lifting Convolution

Since the input height profile is a single-channel image, which is a function $f_{in} : R^2 \to R$, we first lift it to functions on scaling group $G = \left(R_{>0}, .\right) \chi \left(R^2, +\right)$. Group elements $g \in G$ can be parametrized using $x \in R^2$ and $s \in \left(R_{>0}, .\right)$ such that$g = (x, s)$. For such groups, lifting convolution has form

$$f_{out}(x,s) = \left(f_{in} \star \Phi\right)(x) = \int_{y \in Z^2} f_{in}(y) \Phi\left(s^{-1}(y-x)\right) \tag{6}$$

The input is convolved with rotational steerable filters Φ scaled by different factors s. Note that the scaling transformation for the thin film equation in our case is only a change of resolution since the model directly maps the height profile to the temperature profile. This operation is scale-equivariant due to the scale group convolution and rotationally equivariant since the filters Φ are constrained to be steerable.

Group Convolution

After the first lifting layer, both the input and output feature map and filters are now function on G. They now have one additional group dimension defined over$\left(R_{>0}, .\right)$, besides the usual spatial dimensions defined overR^2.The group convolution takes the form,

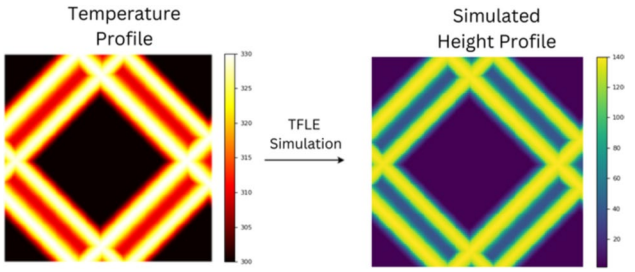

Fig. 3 Thin film lubrication equation simulation for a Diag data sample (data sample from Diag-TFLE dataset)

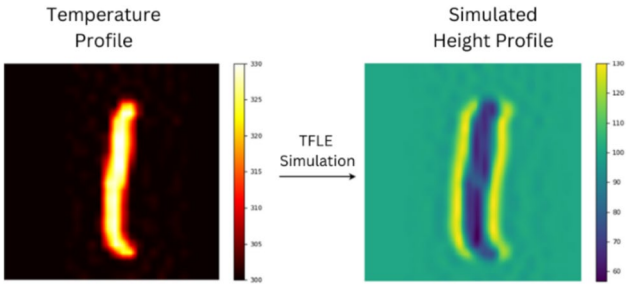

Fig. 4 Thin film lubrication equation simulation for a MNIST data sample (data sample from MNIST-TFLE dataset)

$$f_{out}(x,s) = \left(f_{in} \star \Phi\right)(x,s) = \int_{y \in Z^2} \int_{s' \in (R_{>0},.)} f_{in}\left(y, s'\right) \Phi\left(s^{-1}(y-x), s^{-1}s'\right) \tag{7}$$

Note that the scaling transformation is acting on both the spatial dimensions and the s axis, which indicates a shift by one level up in the scale space. Please refer to [23] for more details. The physical scaling law dictates our model should be equivariant to both up and down scaling and by any $s \in \left(R_{>0}, .\right)$. In practice, the integral over s is approximated by the sum of 5 different scales factors $s \in \{0.5, 0.75, 1, 1.5, 2\}$. Similar to above, this operation is both scale and rotation equivariant.

Experiments

TFLE Simulation and Synthetic Dataset Generation

The experiments necessary for real-world data are expensive. For our proof-of-concept study, we use finite-difference methods to generate a synthetic dataset by simulating the thin film lubrication equation (TFLE) depicted in Eq. 2.

The resolution of both temperature and height profiles is 200×200. The temperature profile consists of peaks of temperatures in random patterns across the thin film after a sufficient amount of time such that the profile has stabilized.

This results in the ridge and trench pattern in the resulting height profile. Temperatures are in Celcius and heights are in nanometers.

We consider two different types of temperature maps resulting in two datasets, one generated by crossing diagonal lines Diag-TFLE (refer Fig. 3) and one generated by the MNIST dataset MNIST-TFLE (refer Fig. 4). We consider MNIST for input signal generation in order to show our method can generalize to natural and real-world input signals. For MNIST, we resize the dataset to 200×200. We use a base temperature of 300 degrees Celsius, varied up to 360 degrees Celsius, and carry out the simulations for a sufficient number of iterations (time) until the height profile has stabilized.

We train and test our models on both of our synthetic datasets. We compare rotationally equivariant versions of *ResNet* and *U-Net* called *RotEq-ResNet* and *RotEq-U-Net*, scale-equivariant steerable network called SESN, and rotation + scale-equivariant network called *RotSc*, with convolution neural network architectures *CNN*, *U-Net*, and *ResNet*. We train and test rotationally equivariant architectures on Diag-TFLE, and all the models are trained and tested on MNIST-TFLE.

Evaluation Metrics

As a metric, we use root mean square error (RMSE) between the predictions and the ground truth over all pixels. We also performed spatial statistics on the error maps between the ground truth and predicted to get pixel accuracy. Pixel accuracy is a metric that quantifies the proportion of correctly predicted pixels in an image, calculated as the ratio of pixels with predicted values exactly matching the ground truth to the total number of pixels.

Experimental Setup

Unless otherwise mentioned, the models are trained for 60 epochs. We use a training set of size 2000, a validation set of size 700, and a test set of size 300. All models were trained on a single 16 GB GPU.

Experiments on Synthetic MNIST-TFLE Dataset

Prediction Performance

Table 1 shows the test set prediction RMSEs and pixel accuracies by all the networks. Figure 5 (a) shows the ground truth and the predicted temperature profiles by all the models for a given height profile (backward modeling). Figure 5 (b) shows the ground truth and the predicted height profiles by all the models for a given temperature profile (forward modeling). All the equivariant models perform better than the non-equivariant models. RotSc achieves the lowest RMSE for forward modeling suggesting that incorporating multiple symmetries from the underlying system into a deep learning model helps it perform better than the models into which only a single symmetry is incorporated. SESN, however, achieves the lowest RMSE for backward modeling with RotSc a close second. RotSc may not outperform due to lack of discriminative information, feature redundancy, and diminished generalization. Alternatively, it could be there is sufficient data such that the rotationally equivariant model can learn scale equivariance, a conclusion supported by the results in the next section.

Sample Efficiency for Backward Modeling

We train the models on the backward modeling task with fewer data samples and test with the same test set as in the previous section to demonstrate the sample efficiency of the equivariant networks. Table 2 shows the test errors of the models for experiments where all.

the models were trained with 80% of the original training set (1600 samples) and with 60% of the original training size (1200 samples).

As shown in Table 2, RotSc performs better compared to the other models when trained with fewer samples. This

Table 1 RMSE and pixel accuracies of CNN, ResNet, U-Net and the RotEq-ResNet, RotEq-U-Net, SESN, Rot + Scale ResNet trained and tested on the MNIST dataset for forward and backward modeling

Config	# Params	Forward modeling test RMSE	Forward modeling pixel accuracy	Backward modeling test RMSE	Backward modeling pixel accuracy
CNN	3.5 M	0.19 ± 0.03	$42.04\% \pm 2$	0.23 ± 0.02	$39.83\% \pm 3$
U-Net	3.6 M	0.18 ± 0.02	$57.18\% \pm 3$	0.27 ± 0.03	$47.51\% \pm 3$
ResNet	3.8 M	0.15 ± 0.03	$61.84\% \pm 2$	0.17 ± 0.03	$63.02\% \pm 3$
RotEq-U-Net	3.6 M	0.12 ± 0.02	$64.27\% \pm 4$	0.14 ± 0.02	$67.55\% \pm 2$
RotEq-ResNet	3.9 M	0.09 ± 0.02	$71.39\% \pm 3$	0.06 ± 0.03	$69.08\% \pm 4$
SESN	3.7 M	0.15 ± 0.02	$66.78\% \pm 2$	$\mathbf{0.06 \pm 0.02}$	$64.48\% \pm 3$
RotSc (Ours)	**3.4 M**	$\mathbf{0.09 \pm 0.02}$	$\mathbf{75.63\% \pm 3}$	0.07 ± 0.03	$\mathbf{72.44\% \pm 2}$

Bold values indicate the better performance of the models for the tasks when compared to the other models that were tested, highlighting the performance of the equivariant neural networks

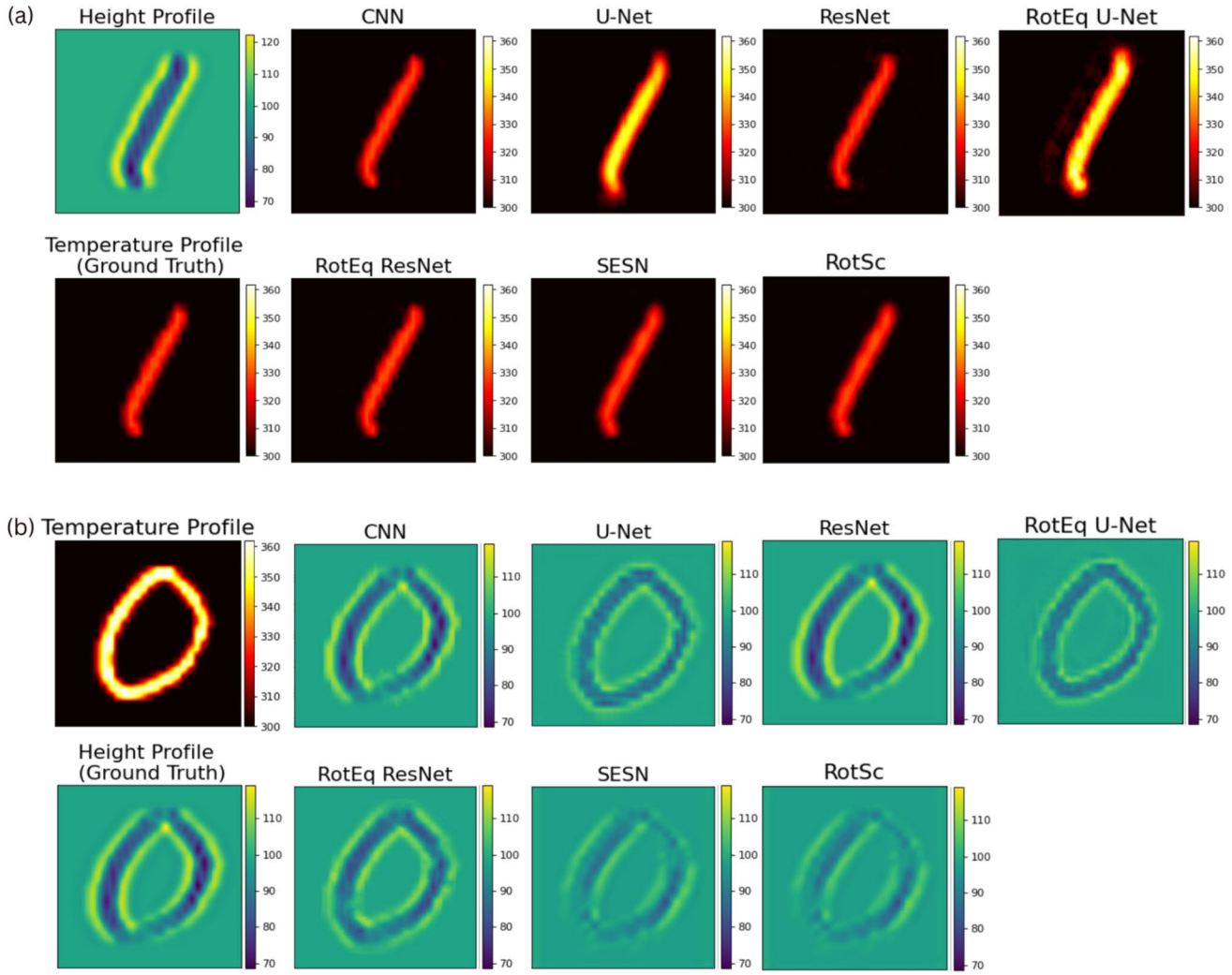

Fig. 5 **a** Height profile, ground truth, and predicted temperature profiles by CNN, U-Net, ResNet, RotEq-U-Net, RotEq-ResNet, SESN, Rot + Scale ResNet (backward modeling). **b** Temperature profile, ground truth, and predicted height profiles by CNN, U-Net, ResNet, RotEq-U-Net, RotEq-ResNet, SESN, Rot + Scale ResNet (forward modeling)

Table 2 Test errors of the models (backward modeling) for the two cases of sampling experiments

Config	80% Train samples	60% Train samples
CNN	0.37 ± 0.03	0.92 ± 0.04
U-Net	0.35 ± 0.03	0.49 ± 0.03
ResNet	0.24 ± 0.02	0.37 ± 0.03
RotEq-U-Net	0.17 ± 0.02	0.28 ± 0.04
RotEq-ResNet	0.15 ± 0.02	0.21 ± 0.03
SESN	0.11 ± 0.03	0.17 ± 0.04
RotSc (Ours)	$\mathbf{0.09 \pm 0.02}$	$\mathbf{0.15 \pm 0.03}$

Bold values indicate the better performance of the models for the tasks when compared to the other models that were tested, highlighting the performance of the equivariant neural networks

shows that a larger symmetry group results in better sample efficiency since learning a given sample means also learning all transformed versions. Exploiting multiple symmetries can enhance the model's ability to learn meaningful representations and generalize well to unseen data.

The mapping from the temperature input to the induced height profile is inherently complex due to the nonlinear nature of the thin film equation, which governs this interaction. Traditional numerical solvers often fail to capture the intricacies of this mapping, leading to inefficiencies and physically unrealistic solutions. Our preliminary attempts with simpler models, including CNN, U-Net, and ResNet without equivariant design, produced results that were poor. These models struggled to preserve the rotational and scale symmetries inherent in the thin film dynamics, resulting in distorted predictions that were not

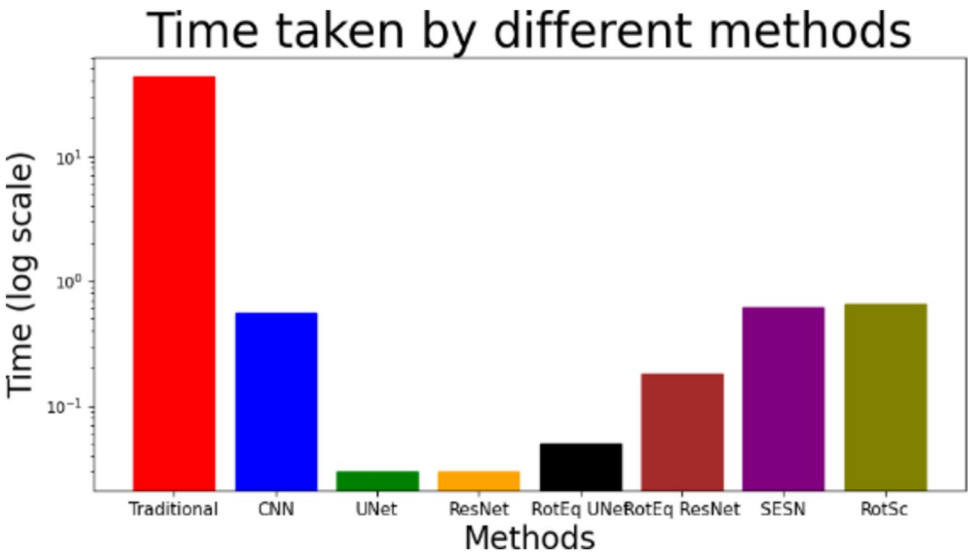

Fig. 6 Time efficiency of deep learning models over traditional methods

physically meaningful. By contrast, our ENNs are specifically designed to respect these symmetries, allowing for more accurate and physically consistent temperature-to-height mappings. The added complexity of ENNs is justified by the significant improvements in prediction accuracy and efficiency, as demonstrated in our baseline comparisons, where ENNs consistently outperformed traditional approaches in both accuracy metrics and computational cost. This highlights the necessity of using ENNs to solve such a highly nonlinear inverse problem in a physically realistic manner.

Time Efficiency

For all the neural networks tested, the inference wall clock time is in the range of a few tenths of a second to predict the temperature profile that can induce a given height profile in the case of backward modeling, and the height profile from a given temperature profile in the case of forward modeling. The data used for this experiment here is a single data sample chosen at random from the test set. The traditional method of solving the partial differential equation takes an average of 43 s to do the same task in the case of forward modeling. This is the time taken to compute the height profile that achieves a steady state for a given temperature profile. Clearly, the deep models are much more time efficient compared to the traditional method of computing. They are faster by a scale of ~ *100x*. Figure 6 shows the inference time comparison between DL models and traditional computing methods on a logarithmic scale.

This time efficiency is crucial when integrating these models with lasers. This will ensure much less of time being utilized in computing the laser pattern required to produce a certain pattern on an SLM. More of this is explained in the 'Path to Deployment' section.

Path to Deployment

One key advantage of thermocapillary SLMs is that they are compatible with high-power lasers. Laser thermocapillary dewetting (TC) can be applied to a host of nano-manufacturing applications, including the creation of advanced optics and the rapid prototyping of electrodes for lab-on-chip applications.

When a collimated laser beam is transmitted through a lens, the resulting pattern at the focal plane is related to the Fourier transform of the original intensity distribution. Our AI models help in accelerated prediction of the pattern of the laser bean required to produce a certain pattern at the focal plane, instead of having to compute it using Fourier transforms. When these models are directly integrated for usage with the lasers, patterns in the SLM can be cycled through without having to exhaust too much of the time and computing resources. This can be done by integrating it as a computer vision system into automated experimentation systems like ARES (autonomous research system) [32]. The neural models are small enough to run on single GPU systems and hence can be integrated into deployed systems to provide real-time control. But some engineering challenges do exist

before deployment, which includes making sure that the training dataset has good enough coverage to ensure good generalization to desired patterns at runtime.

Conclusion

We develop methods to improve the performance of deep learning models for learning the relationship between a height profile and a corresponding temperature profile of

a dynamic spatial light modulator. We incorporate various symmetries by designing equivariant neural networks and demonstrate their superior performance on prediction for both forward and backward modeling experimentally. To the best of our best knowledge, there does not exist a single model with equivariance to the full symmetry group of the thin film equation apart from ours.

Funding National Science Foundation, 2107256, Robin Walters, 2134178, Robin Walters

References

1. Zhang X, Wang L, Helwig J, Luo Y, Fu C, Xie Y et al (2023) Artificial intelligence for science in quantum, atomistic, and continuum systems. arXiv preprint arXiv:2307.08423
2. Wang R, Yu R (2021) Physics-guided deep learning for dynamical systems: a survey. arXiv Preprint arXiv:2107.01272
3. Strogatz SH (2018) Nonlinear dynamics and chaos: with applications to physics, biology, chemistry, and engineering. CRC press
4. Izhikevich EM (2007) Dynamical systems in neuroscience. MIT press
5. Bartoldson B, Wang R, Fu Y, Widemann D, Nguyen S, Bao J et al (2022) Latent space simulation for carbon capture design optimization. Proceedings of the AAAI conference on artificial intelligence. pp 12447–12453
6. Wei J, Chu X, Sun X-Y, Xu K, Deng H-X, Chen J et al (2019) Machine learning in materials science. InfoMat 1:338–358
7. Choudhary K, DeCost B, Chen C, Jain A, Tavazza F, Cohn R et al (2022) Recent advances and applications of deep learning methods in materials science. npj Computational Maters 8:59
8. Gilmer J, Schoenholz SS, Riley PF, Vinyals O, Dahl GE (2017) Neural message passing for quantum chemistry. In: International conference on machine learning. PMLR, pp 1263–1272
9. Hoogeboom E, Satorras VG, Vignac C, Welling M (2022) Equivariant diffusion for molecule generation in 3d. In: International conference on machine learning. PMLR, pp 8867–8887
10. Kovacevich DA, Ma T, Gamboa AR, Nitzsche MP, Saro-Cortes V, Davis E et al (2021) Thermocapillary dewetting-based dynamic spatial light modulator. Opt Lett 46:3721–3724
11. Thomson J (1855) XLII. On certain curious motions observable at the surfaces of wine and other alcoholic liquors. Lond, Edinb, Dublin Philos Mag J Sci 10:330–333
12. Bénard H (1900) Les tourbillons cellulaires dans une nappe liquide. Revue Gen Sci Pure Appl 11:1261–1271
13. Bénard H (1901) Les tourbillons cellulaires dans une nappe liquide - Méthodes optiques d'observation et d'enregistrement. J Phys Theor Appl 10(2):54–66
14. Wang X-B, Tian S-F (2018) Lie symmetry analysis, conservation laws and analytical solutions of the time-fractional thin-film equation. Comput Appl Math 37:6270–6282
15. Weiler M, Cesa G (2019) General E(2)-equivariant steerable cnns. In: Advances in Neural Information Processing Systems, vol 32
16. Darhuber AA, Troian SM (2005) Principles of microfluidic actuation by modulation of surface stresses. Annu Rev Fluid Mech 37:425–455
17. Cherniha R, Myroniuk L (2010) Lie symmetries and exact solutions of a class of thin film equations. J Phys Math 2:1–19
18. Charalambous K, Sophocleous C (2013) Symmetry properties for a generalised thin film equation. J Eng Math 82:109–124
19. Tompson J, Schlachter K, Sprechmann P, Perlin K (2017) Accelerating eulerian fluid simulation with convolutional networks. In: Proceedings of the 34th international conference on machine learning. vol 70. JMLR, pp 3424–3233
20. Sanchez-Gonzalez A, Godwin J, Pfaff T, Ying R, Leskovec J, Battaglia P (2020) Learning to simulate complex physics with graph networks. arXiv:2002.09405
21. Wang R, Kashinath K, Mustafa M, Albert A, Yu R (2020) Towards physics-informed deep learning for turbulent flow prediction. In: Proceedings of the 26th ACM SIGKDD international conference on knowledge discovery & data mining, pp 1457–1466
22. Cohen T, Welling M (2016) Group equivariant convolutional networks. In: International conference on machine learning. PMLR, pp 2990–2999
23. Worrall D, Welling M (2019) Deep scale-spaces: Equivariance over scale. In: Advances in Neural Information Processing Systems, vol 32
24. Worrall DE, Garbin SJ, Turmukhambetov D, Brostow GJ (2017) Harmonic networks: deep translation and rotation equivariance. In:Proceedings of the IEEE conference on computer vision and pattern recognition, pp 5028–5037
25. Weiler M, Hamprecht FA, Storath M (2018) Learning steerable filters for rotation equivariant CNNs. Computer Vision and Pattern Recognition (CVPR)
26. Sosnovik I, Szmaja M, Smeulders A (2019) Scale-equivariant steerable networks. arXiv preprint arXiv:1910.11093
27. Wang R, Walters R, Yu R (2020) Incorporating symmetry into deep dynamics models for improved generalization. arXiv preprint arXiv:2002.03061
28. Smidt TE (2021) Euclidean symmetry and equivariance in machine learning. Trends Chem 3:82–85
29. Simm GNC, Pinsler R, Csányi G, Hernández-Lobato JM (2021) Symmetry-aware actor-critic for 3D molecular design. International conference on learning representations [Internet]. https://openreview.net/forum?id=jEYKjPE1xYN
30. Sosnovik I, Szmaja M, Smeulders A (2020) Scale-equivariant steerable networks. In: International conference on learning representations [Internet]. https://openreview.net/forum?id=HJgpugrKPS
31. Cesa G, Lang L, Weiler M (2022) A program to build E(N)-equivariant steerable CNNs. In: International conference on learning representations [Internet]. https://openreview.net/forum?id=WE4qe9xlnQw
32. Stach E, DeCost B, Kusne AG, Hattrick-Simpers J, Brown KA, Reyes KG et al (2021) Autonomous experimentation systems for materials development: a community perspective. Matter 4(9):2702–2726